ELSEVIER

Journal of Contaminant Hydrology 31 (1998) 315–335

JOURNAL OF
Contaminant
Hydrology

Rapid fluid content measurement method for fingered flow in an oil–water–sand system using synchrotron X-rays

Alon Rimmer [a], David A. DiCarlo [a], Tammo S. Steenhuis [a,*], Barnes Bierck [a], Deanna Durnford [b], J.-Yves Parlange [a]

[a] *Department of Agricultural and Biological Engineering, Cornell University, Ithaca, NY 14853, USA*
[b] *Department of Chemical and Bioresource Engineering, Colorado State University, Ft. Collins, CO 80523, USA*

Received 12 August 1997; accepted 28 August 1997

Abstract

The complexity of simultaneous flow of water and non-aqueous phase liquids is largely unappreciated because few techniques permit accurate quantitative measurement of water and oil contents in rapidly changing flow fields. High intensity X-rays were used at the Cornell High Energy Synchrotron Source (CHESS) to obtain rapid, accurate, and non-destructive quantitative measurements of the changing fluid contents in a porous medium during infiltration events. Concomitant temporal pressure measurements were obtained for each liquid phase using rapidly responding tensiometers. The system was used for measuring temporal volumetric fluid content changes during a water finger infiltration into sand saturated with a NAPL (Soltrol-220) in a two-dimensional chamber. The fluid content distribution of a finger in the oil–water system was found to be similar to air–water systems. The hysteretic constitutive relationship between pressure and the content was developed from the data. The relationship was used to explain why the finger did not widen behind the tip, and why, upon re-infiltration, water followed the previously established path. These findings are relevant for cleanup of oil-contaminated sites because it aids in the understanding of hydrologic control which is an essential component of cost-effective in-situ remediation. © 1998 Elsevier Science B.V.

Keywords: Oil–water–sand system; Synchrotron X-rays; Water-finger infiltration

* Corresponding author.

PII S0169-7722(97)00070-3

1. Introduction

Groundwater contaminants are introduced at or near the soil surface via spills, leakage from fuel tanks, or overfilling of tanks. Many of these contaminants are organic compounds of low water solubility, existing as separate liquid phases in soil pore spaces (Dane et al., 1992). The problem is severe. For example, the volume of contaminants at 130 Department of Energy (DOE) facilities alone exceeds 2500 billion liters (Department of Energy, 1995; Wilkins et al., 1995). The anticipated life-cycle cleanup costs are expected to be greater than US$300 billion and will take at least 100 years using existing technologies.

In-situ remediation technologies are the only viable approaches with potential for controlling the huge costs and extended times required to clean up these sites. However, cleanup procedures are often instituted and operated with limited knowledge of both the physical and chemical processes governing contaminant transport (Wilkins et al., 1995). To be effective complete hydrologic control of the subsurface at the remediation site is critical. Hydrologic control at NAPL contaminated sites can be improved by better knowledge of rapidly changing flow fields (Mercer and Cohen, 1990). The flow fields can be studied in the laboratory by accurately measuring water and oil contents in 2-d chambers.

Early observations of oil and water flow were made in Hele–Shaw flow cells by Saffman and Taylor (1958) and Chuoke et al. (1959). Currently, most real-time, non-intrusive measurements of oil and water contents in porous media are made using gamma- and X-ray attenuation techniques. For example, a dual-energy gamma radiation method was described by Hopmans and Dane (1986), and was applied to study saturation changes during monotonic liquid drainage (Lenhard et al., 1988; Dane et al., 1992). The X-ray absorption (film-based radiography) technique described by Tidwell and Glass (1994) can be used to obtain full field oil and water contents. However, the conventional X- and gamma-ray methods are limited by the relatively low intensity of Am 241, Cs 137, and X-ray tube sources, which do not permit accurate monitoring of flow phenomena occurring in porous media on temporal scales of seconds.

Other methods for determining oil and water fluid contents, which permit the measurement of rapidly changing flow fields, are the full-field visualization techniques described by Van Geel and Sykes (1994) and Darnault et al. (1998). They involve dying the fluids and analyzing visual information with computer graphics techniques. Van Geel and Sykes (1994) dyed the oil red and analyzed the reflected light. They determined the fluid contents near the glass wall which may not represent that of the chamber. Darnault et al. (1998) colored the water with 0.005% blue dye and recorded the transmitted light from a bank of high-frequency fluorescent lights behind the slab chamber. The color (or hue) of the images was related to moisture-content values. However, scattering near the edges made it more difficult to see sharp boundaries. Moreover, the sands need to be translucent (Tidwell and Glass, 1994). While light transmission techniques allow monitoring of many array points in a relatively large two-dimensional section of a soil slab, X-ray attenuation permits more accurate water-content measurements in a small section of any soil type.

A final destructive method for visualizing oil and water contents is by using oils that solidify. After solidification, the columns are sectioned and the distribution of oil studied (Conrad et al., 1992; Powers et al., 1992).

The objective of this paper is to present a method using synchrotron X-rays that allows rapid quantitative, and precise measurements of fluid contents in oil–water systems. Synchrotron radiation can be up to 10,000 times as intense than conventional X-ray sources, which decreases errors and counting times. Synchrotron beam lines are rapidly increasing and are available to the general scientific community.

To illustrate the application of the synchrotron X-ray technique, we experimented with fingered water flow through a sand initially saturated with a light oil (Soltrol 220). Soltrol has negligible water solubility, very low volatility at room temperatures, and poses a low health hazard. We measured fluid contents and pressures in both phases using phase-sensitive tensiometers. This study is relevant because fingered flow generated by chaotic disturbances in a flow field is one of the factors complicating hydrologic control during in-situ cleanup, and can render the use of in-situ treatment remedies ineffective because of hydrodynamic bypassing of subsurface pollutants. With the result of the synchrotron experiments, the forming and persistence of these bypass flow paths are explained. It is shown that because of hysteresis in the constitutive relationships, these paths are in equilibrium with the surrounding oil fluid. Finally, the synchrotron and other measurements are used to scale the finger diameter. By taking soil and fluid properties into account we calculate the dimensions of the bypass flow paths.

2. Background

2.1. Unstable flow phenomena

Instabilities involving two immiscible fluids (known as bypass flow) have been observed in the oil industry for some time (Craft and Hawkins, 1959). General stability criteria for two liquids have been given by Saffman and Taylor (1958) and Chuoke et al. (1959) and specific criteria for air–water systems in soil by Parlange and Hill (1976), Raats (1973), Philip (1975), and Hillel and Baker (1988). In general, the flow will be unstable if the pressure difference between the two liquids is greatest where the fluid has intruded the farthest. This condition can be met when a less viscous fluid intrudes into a more viscous fluid, and/or when a denser fluid intrudes with gravity into a less dense fluid.

Diameters of fingers in air–water systems, $d_{a/w}$, were calculated by Parlange and Hill (1976), Glass et al. (1989a,b), and Liu et al. (1994a). The equation based on Parlange and Hill (1976) and simplified by Liu et al. (1994a) applies to well sorted sands (i.e., those with narrow particle-size distributions) where the slope of the wetting branch of the soil characteristic curve, $\mathrm{d}h_{a/w}/\mathrm{d}\theta_w$, is straight over the portion where $K(\theta)$ decreases rapidly with decreasing moisture content, viz:

$$d_{a/w} \simeq \frac{2\kappa\theta_f\left(\dfrac{\mathrm{d}h_{a/w}}{\mathrm{d}\theta_w}\right)}{\eta + 1.5} \tag{1}$$

where κ is 4.8 for three-dimensional fingers (Glass et al., 1990) and θ_f is the moisture content at the finger tip. In case fingers are constrained to two dimensions in laboratory chambers κ is equal to π. η may be found as (Brooks and Corey, 1964):

$$\eta = \frac{2}{\lambda} + 3 \tag{2}$$

where λ is a positive index related to the pore size distribution of soil with values ranging from 2 to 7 resulting in η values between 3.3 and 4.

Based on Hele–Shaw type of experiments, finger width for two-phase immiscible oil-water systems, $d_{o/w}$, was given by Chuoke et al. (1959), who assumed that a relationship, analogous to the Laplace–Young relationship, exists between the macroscopic frontal curvature and the pressure jump across the front as (Glass et al., 1991b):

$$d_{o/w} = \kappa \left[\frac{3\sigma^*}{g(\rho_w - \rho_o)\left(1 - \frac{q}{K_{w_f}}\right)} \right]^{0.5} \tag{3}$$

where g is the gravity, ρ_w is specific weight of water, ρ_o is specific weight of oil, q is flux, and K_{w_f} is the conductivity in the finger. A difficulty with Eq. (3) is the 'effective' surface tension σ^* which has not been defined, although Homsy (1987) associated it with a modified capillary number.

Chandler et al. (1997) assuming little resistance to moving of the oil, related the fingers in oil-water and air-water systems as:

$$\frac{d_{o/w}}{d_{a/w}} = \frac{\frac{\sigma_{o/w}}{\sigma_{a/w}}}{1 - \frac{\rho_o}{\rho_w} - \frac{q}{K_{w_f}}} \tag{4}$$

where the σ's are the surface tension for fluid pairs and includes the contact angle effects. Noticing that the K_{w_f} is usually close to the saturated conductivity (Selker et al., 1992b) (Glass et al., 1989b), we can often neglect the term q/K_{w_f} with respect to $(1 - \rho_o/\rho_w)$. Then, because the matric potential between fluid pairs scale as the surface tension (Parker and Lenhard, 1987), we find by combining Eqs. (1) and (4):

$$d_{o/w} = \frac{2\,\kappa\,\theta_f \frac{dh_{o/w}}{d\theta_w}}{\left(1 - \frac{\rho_o}{\rho_w}\right)(\eta + 1.5)} \tag{5}$$

where the $dh_{o/w}/d\theta_w$ is the slope of the wetting part of the oil–water characteristic curve. For very low infiltration rates, the slope may change (Yao and Hendrickx, 1996) and the more complete equation of Parlange and Hill (1976) needs to be used.

3. Scaling of finger diameter

Eq. (3), assuming that σ^* scales like the surface tension, and Eq. (5) predict different finger scaling behavior with fluid density, fluid interfacial tension, and the coarseness of the porous medium. In the following analysis we will compare widths of slow moving fingers and, thus, minimize the effects of the flux dependency. Noting that matric potential scales as the inverse of the microscopic length (Miller and Miller, 1956), we can also write the finger scaling in the form:

$$d = d^* c \left[\frac{D_{50}^*}{D_{50}} \frac{G^*}{G} \frac{\sigma_{\mathrm{nw}}}{\sigma_{\mathrm{nw/w}}^*} \right]^b \tag{6}$$

where the superscript * is the 'reference soil with reference fluids', $G = (1 - \rho_{\mathrm{nw}}/\rho_{\mathrm{w}})$ and accounts for different fluid densities, and D_{50} is mean particle diameter. The subscript w is for wetting and subscript nw for nonwetting. The coefficient, b, equals 1 for scaling according to Eq. (4) and b is 0.5 using Eq. (3) of Chuoke et al. (1959). The factor c is a correction factor for difference in moisture content in the finger tip and type of chamber used (2 or 3 dimensional). By introducing scaling factors for the particle size, f_D, for gravity, f_G, and surface tension, f_σ, Eq. (6) can be rewritten as:

$$d = c[\, f_D\, f_G\, f_\sigma \,]^b\, d^* \tag{7}$$

where

$$f_D = \frac{D_{50}^*}{D_{50}} \tag{8}$$

$$f_G = \frac{G^*}{G} \tag{9}$$

$$f_\sigma = \frac{\sigma_{\mathrm{nw/w}}}{\sigma_{\mathrm{nw/w}}^*} \tag{10}$$

$$\begin{aligned} c &= c_\theta c_\kappa \\ c_\theta &= \frac{\theta_{\mathrm{f}}}{\theta_{\mathrm{f}}^*} \\ c_\kappa &= \frac{\kappa}{\kappa^*} \end{aligned} \tag{11}$$

In Eq. (11) κ is the coefficient introduced by Glass et al. (1990), for 2–d ($\kappa = \pi$) and for 3–d ($\kappa = 4.8$). The correction for moisture content in the finger tip, c_θ is based on fluid content measurements. The effect of the moisture content on the finger is not specified in Chuoke's Eq. (3). The correction factor tends to be small and, therefore, the high precision is not necessary.

3.1. Oil and water content measurement using synchrotron X-rays

Bierck et al. (1988) described a method using synchrotron radiation to monitor consolidation of clays under seepage stress. The high intensity of synchrotron radiation permits acquisition of transmitted X-ray intensities through relatively thick regions (on the scale of centimeters) during short time intervals (in a second or less). This method was adapted, as described by Liu et al. (1993), to measure water-content changes during rapid water finger movement through sand.

In a two-fluid system, such as oil and water, the water content can be directly related to the attenuation of the X-rays, $\ln(I/I_0)$, where I and I_0 are the transmitted and incident radiation intensities, respectively. Straightforward calculations (Liu et al., 1993; Lenhard et al., 1988) yield the water content in terms of the measured X-ray attenuation, as:

$$\theta_w = \frac{\ln\left(\frac{I}{I_0}\right) - \ln\left(\frac{I_{sat}}{I_0}\right)}{(\alpha_o - \alpha_w)\,x}. \tag{12}$$

Here θ_w is the volumetric water content (cm^3/cm^3), I_{sat} is the transmitted intensity through the initially oil-saturated porous media, x is the thickness of the chamber (cm), and α_w and α_o are the attenuation coefficients (cm^{-1}) for the water and oil. The volumetric oil content θ_o is given by:

$$\theta_o = n - \theta_w, \tag{13}$$

where n is the porosity.

4. Materials and methods

Experiments were carried out at the F-2 beam line of the Cornell High Energy Synchrotron Source (CHESS), which provides an intense, high energy X-ray beam (Batterman and Ashcroft, 1979). Using a Si(311) monochromator, the beam's energy was tuned to 33.2 keV. This energy level was chosen because it was slightly above the iodine absorption edge and increased the contrast between oil and water doped with 30 g l^{-1} of potassium iodide. Subsequently, the beam passed through a set of slits, a sealed Xe ionization chamber, the sample chamber, and another sealed Xe ionization chamber. Ionization chambers produce a current directly proportional to the X-ray intensity that passes through them. The slits defined a beam cross-section of 0.1 cm high and 0.6 cm wide. For each ion chamber, the current was converted into a frequency, and acquired by a computer which automatically recorded the relative incident and transmitted radiation. The sample chamber was mounted on a computer controlled translation stage, allowing monitoring of fluid content changes at different positions within the chamber.

The sand slab, illustrated in Fig. 1, was a chamber 54 cm high, 23 cm wide, and 0.95 cm thick with 0.95 cm polycarbonate walls, equipped with four water and four oil

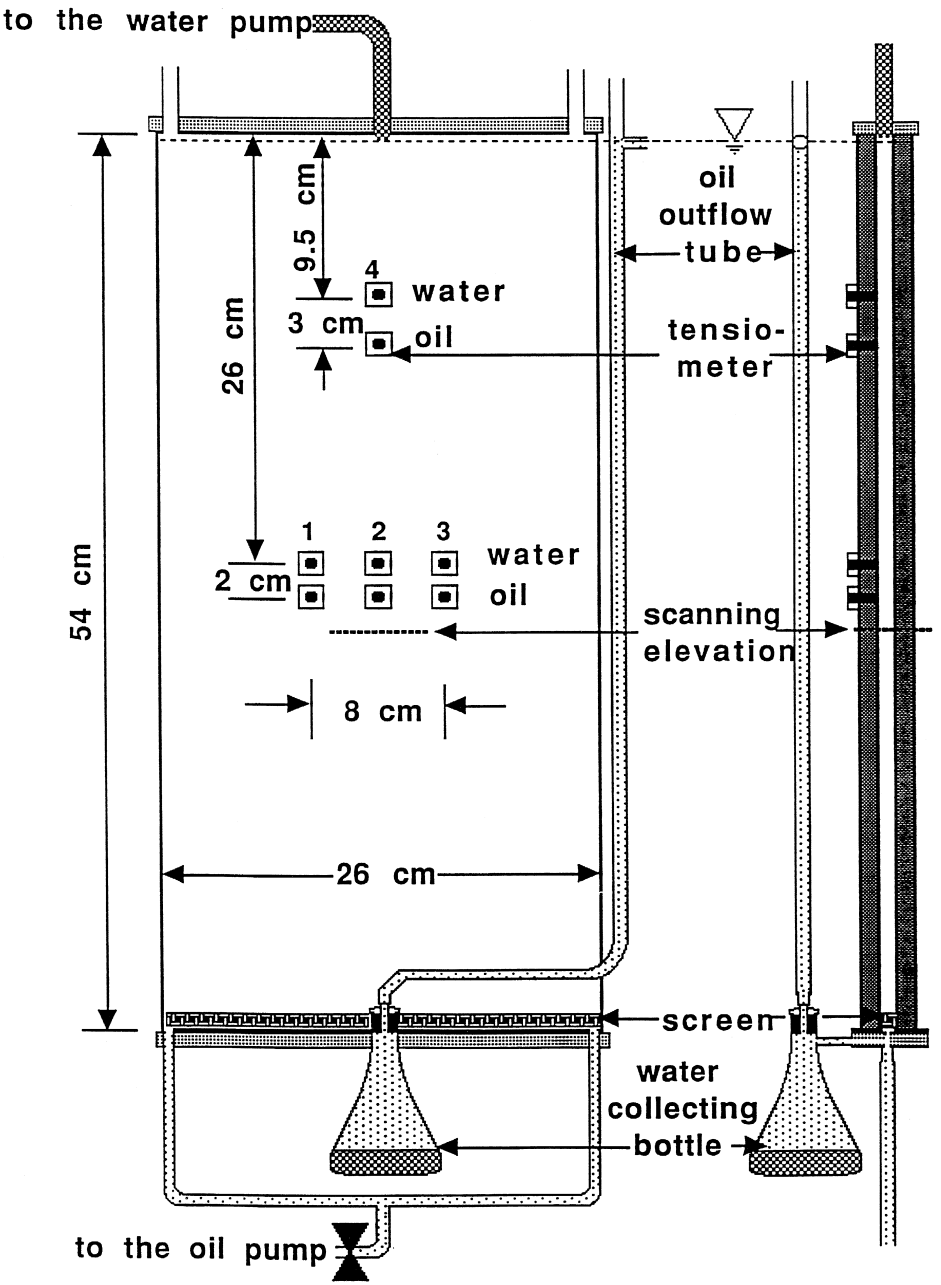

Fig. 1. Front and side view of the experimental chamber. There was one set of top tensiometers and three sets of middle tensiometers. Water contents were measured at the scanning elevation, directly below the middle tensiometers. The bottle and the outflow tube were used to keep the oil pressure constant during water infiltration.

tensiometer ports. The chamber was positioned vertically such that the X-rays struck (and thus, monitored the fluid contents) 2 cm below the lower oil tensiometers and 30 cm below the top of the chamber. This initial position is indicated by a dotted line in Fig. 1.

Two types of sieved silica sand were used to pack the chamber; either '20/30 sand' or '12/20 sand' with grain diameters between 0.59–0.85 mm and 0.85–1.5 mm, respectively. Soltrol 220, a mixture of alkanes C13 through C17 (Phillips 66), provided the oil phase for the experiments. Distilled water doped with potassium iodide at 30 g l^{-1}, and colored blue with FD and C Blue #1, provided the aqueous phase. The potassium iodide increased the X-ray attenuation of the aqueous phase, and the blue food coloring allowed a visual inspection of water position.

Oil- and water-specific tensiometers were developed by modifying high-speed tensiometers (Selker et al., 1992a) to measure oil (ψ_o) and water (ψ_w) pressures. The matric potential is the difference of the oil and water pressure measurements. The interiors of the oil tensiometers were filled with oil while a hydrophobic plastic porous plate (0.8 cm diameter) provided the connection to the sand. The water tensiometers used a 0.8-cm-diameter porous glass plate with relatively large pores. The oil tensiometers and their connections are illustrated in Fig. 2. A three-way valve connected pressure transducers

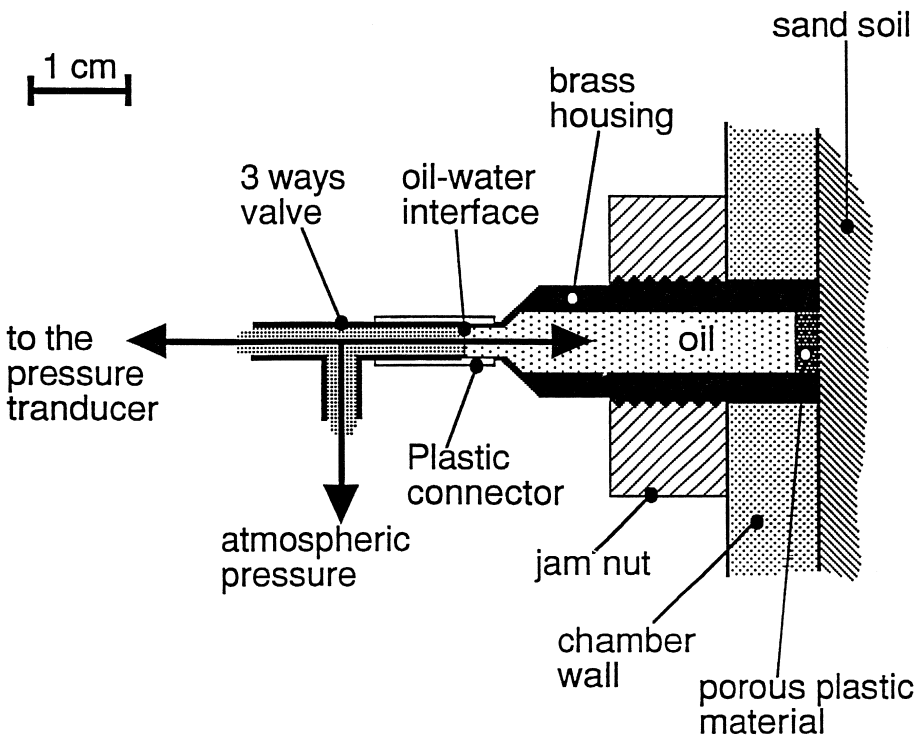

Fig. 2. Close-up view of an oil tensiometer inserted into the chamber. Water tensiometers were completely filled with water and used a ceramic porous plate.

to either a tensiometer or the atmosphere, enabling readings of reference pressures during experiments. Each transducer output was amplified, converted into a frequency, and captured by a data acquisition system. Calibration of the readings into centimeters of water was achieved by recording the transducer output under a sequence of measured water column heights. During the experiments, the pressure data were recorded simultaneously with the X-ray intensity measurements.

5. Experimental procedure

Initially the constants in Eqs. (12) and (13) (x, n, α_w, and α_o), were measured. The thickness of the chamber, x, was determined using a dial caliper, and the porosity was calculated from the volume of oil required to saturate a given volume of the packed soil slab.

The attenuation constants α_w and α_o were determined using the method described by Lenhard et al. (1988). A polycarbonate standard cell with five sequential, 0.5-cm-thick compartments was employed. X-ray attenuation was measured for the (empty) standard cell after each compartment was sequentially filled with either water or oil. A linear regression of the attenuations yielded the attenuation constants for the two fluids. This procedure was repeated several times throughout the experimental period to verify the stability of the standards and the beam.

Six separate finger experiments were conducted using two sieved sand types and three water infiltration rates (Table 1). As we were interested in testing both the changing fluid contents vs. time within the finger, and the fluid contents in a horizontal cross section of the finger, X-ray attenuation measurements were collected in two different manners. The first consisted of measuring the attenuation at one particular position versus time, the second consisted of measuring the attenuation versus the horizontal position of the chamber. In a typical experiment, most of the time was spent observing fluid changes within the finger boundaries, with periodic checks of how the finger cross section had changed. The tensiometer data were taken at all times.

Using a peristaltic pump, the sand was saturated from the bottom with oil. Once the chamber was filled with oil, water was infiltrated through a point source at the top of the

Table 1
Synchrotron experiments

Experiment	Sand type	Initial application rate ($cm^3\ mm^{-1}$)	Finger width (cm)	Moisture content in tip (cm^3/cm^3)
I	20/30	1.0	4–7	0.27
II	20/30	2.3	3.5–7	missed
III	20/30	3.8	5–9	0.30
IV	12/20	1.0	2–4	0.30
V	12/20	2.3	2.5–4	0.27
VI	12/20	3.8	2–4	0.20

chamber. A closed drainage system, described below, maintained a relatively constant oil level and pressure even as the water displaced the oil. A nalgene tube connected the bottom of the chamber to the side of an oil-filled drainage bottle (Fig. 1). Another tube connected the top of the drainage bottle to a T-fitting set at the height of the chamber oil level. As water displaced the oil, the excess oil drained through the bottom of the chamber and out through the T-fitting, keeping the oil level constant. The experiment ended when water displaced all the oil in the collecting bottle, thus filling the exit tube with water and raising the oil pressure.

The applied water initially spread both horizontally and vertically while at the top of the chamber, but soon a water finger formed and moved slowly down the chamber. In the coarse 12/20 sand the finger moved straight down, while in the finer 20/30 sand its path tended to meander slightly sideways. During re-infiltration episodes the water followed its previous path down through the chamber.

Relative pressure measurements at CHESS were found to have an accuracy of 0.1 cm of water, but absolute pressures were found to be much less accurate (approximately 5 cm of water). In order to improve the overall accuracy, the experiments were repeated without using the X-ray technique under the same conditions in the Soil and Water Laboratory to determine absolute pressures in the fingers. These experiments showed identical relative pressure changes, but also provided absolute pressures accurate to 1.0 cm of water. Thus, pressure data taken simultaneously with the X-ray data were offset to match the absolute pressures obtained from the concomitant experiments. In these experiments we also measured size and shape of the fingers.

6. Results and discussion

The observations of the distribution of the fluid contents and pressure in the fingers is shown first because it allows us to illustrate the utility of the synchrotron X-rays for documenting the relatively fast moving unstable flows. Then we will show how these measurements can be used to obtain the hysteretic constitutive relationships that explain why fingers are persistent and how fingers scale for Miller similar soils (Miller and Miller, 1956).

6.1. Observations

Table 1 shows the diameter and moisture content in the finger tips for the six synchrotron experiments. The porosity of the sand was 0.36. The oil and water content values in the tip of the fingers for the 12/20 sand obtained with the synchrotron experiment compared well with those obtained with the light transmission technique of Darnault et al. (1998). To our knowledge there are no other measurements available for comparison purposes of fluid contents in rapidly moving oil–water fingers.

Although in each of the six synchrotron experiments accurate measurements of the oil and water contents in the fingers were obtained, both sets of tensiometers were contacted

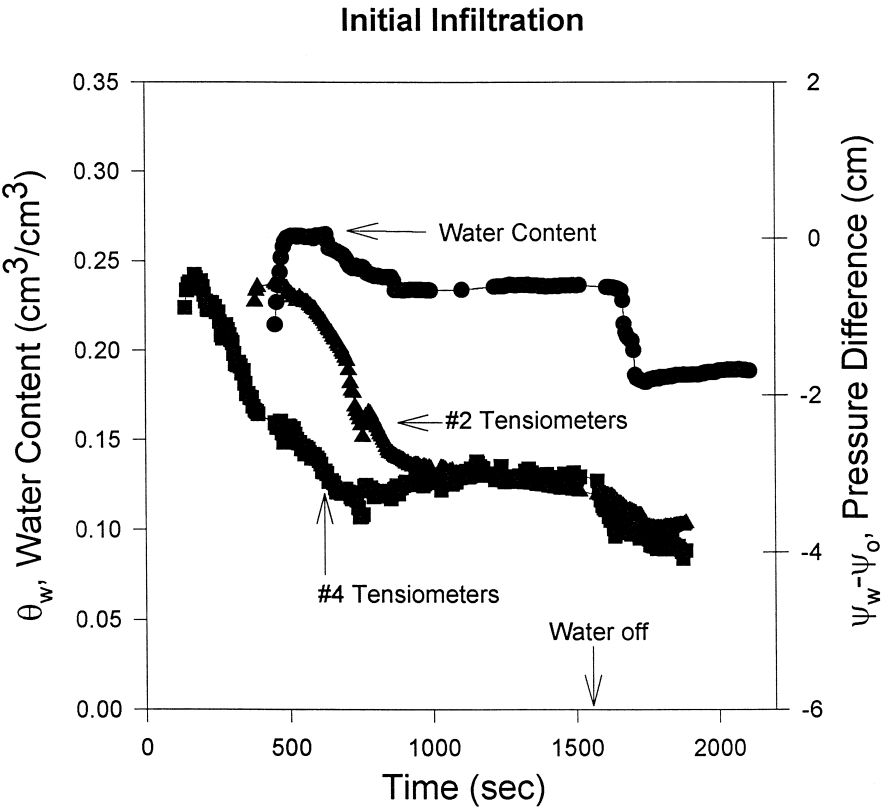

Fig. 3. Water content and pressure measurements as the initial finger moved down the chamber through oil-saturated 12/20 sand. Both water content and pressure rose abruptly at the front of the finger, and fell behind the finger tip, indicative of unstable flow. The water was turned on at $t = 0$ s. When the water was turned off at $t = 1500$ s, both readings dropped again.

by the water finger in only one of the experiments (#5). The water infiltration and (re-infiltration) rate was 2.3 ml min^{-1}. The finger, 3–4 cm in width, formed and moved down the chamber, contacting the #4 and #2 sets of tensiometers (Fig. 1). Fig. 3 shows the temporal changes in water content and capillary potential ($\psi_w - \psi_o$) during the first infiltration. The passage of the finger can be seen in the time delays between the response of the #4 and #2 sets of tensiometers. Also, the water content readings were obtained about 50 s later than the #4 water tensiometer reading. The pressures and water content values exhibit behavior typical of fingers and unstable flow as observed in water–air systems by Selker et al. (1992b); the water content rises abruptly, levels off temporarily, and then drops to a constant value when the finger hits the bottom of the chamber at around 1000 s. When the water was turned off at approximately 1500 s, the water content underwent another abrupt drop as the water drained to the bottom and was replaced by oil. The tensiometer readings also show the typical behavior of unstable

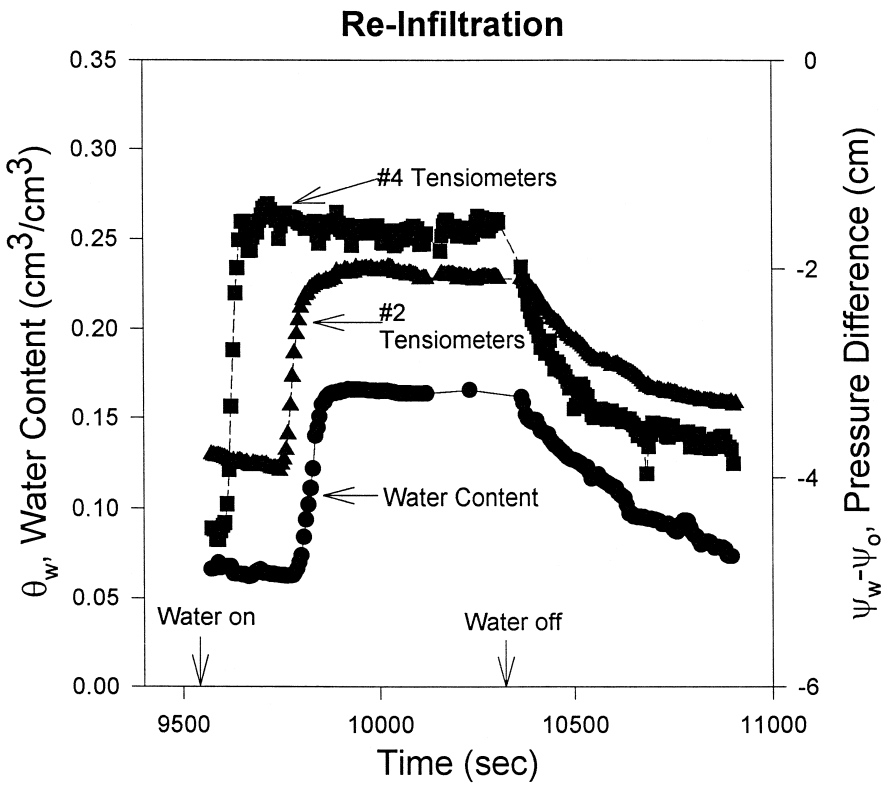

Fig. 4. Water content and pressure measurements during a re-infiltration of the finger. No drops in content or pressure are observed while the water is on, indicating that the re-infiltration is now in a stable flow pattern.

flow in which the matric potential decreases behind the front. Also, after the water was turned off the matric potential dropped even further.

Fig. 4 shows the temporal changes in water content during a re-infiltration episode. In contrast to the initial infiltration, neither the water content nor the pressure difference decreased until the water was turned off. The flow within the original finger boundaries does not show the characteristic drop of pressure behind the finger tip and has characteristics similar to a 'standard' wetting front (i.e., when water infiltrates in a soil with a horizontal wetting front) in which the matric potential increases at the front and then remains relatively constant behind the wetting front. Also, the time delays between the tensiometer and water readings is much less than was observed in the initial infiltration (Fig. 3), showing a much quicker passage of the pulse. All re-infiltration episodes exhibited identical behavior although they are not reported here.

Fig. 5 shows a partial horizontal profile at selected times during the infiltration and re-infiltration cycles. The profile extends from about the middle to the outside of the finger, depicting the wide variation of water contents at the same height. The horizontal boundary over which the moisture content drops in the finger is about 8–10 mm wide, but the actual boundary is likely much smaller than this, as much of the measured width

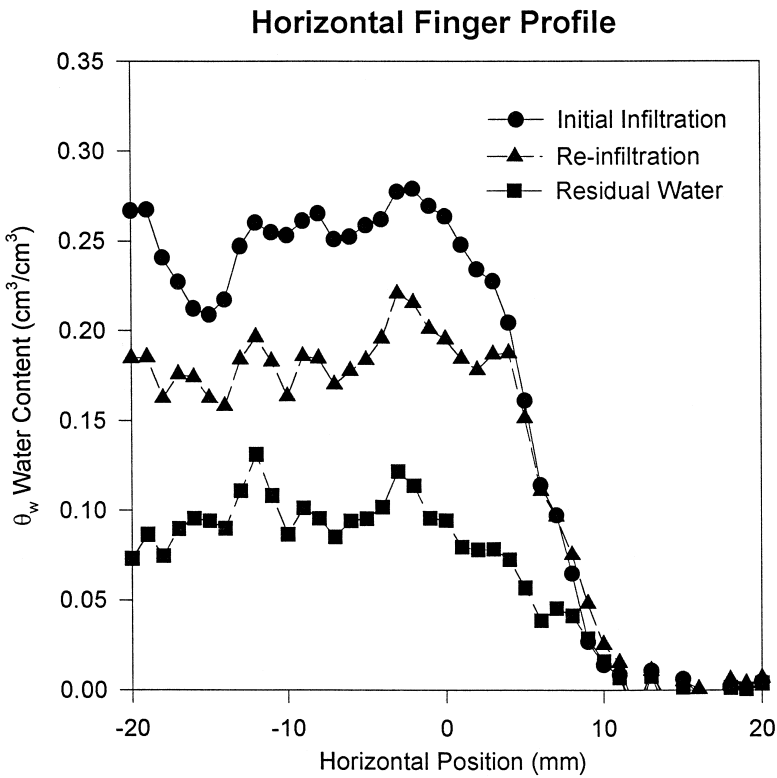

Fig. 5. Horizontal profile of the water content for right-hand side of the finger. (Left-hand side was not measured.) There is no increase in finger size for re-infiltration events.

is due to the fact that the X-ray beam was 6 mm wide. In addition, the boundary (and, thus, the width of the finger) did not change measurably during re-infiltration episodes. Note that this follows the air–water finger observations in which during re-infiltration the finger width remains the same and the moisture content is lower (Glass et al., 1989a,b; Selker et al., 1992b).

6.2. Persistence

Most of the theories of unstable flow have been focused on the instability itself. Persistence of fingers over time, especially in oil–water systems, has received only little attention as noted by Glass and Nicholl (1996). In air–water systems the hysteretic nature of the constitutive relationship has been crucial to understanding the finger persistence (Glass et al., 1989c; Liu et al., 1994b). We will show here that for oil–water systems hysteresis plays much the same role.

The synchrotron data presented above allows us to construct for oil–water systems the constitutive relationship between the fluid pressure difference and water content.

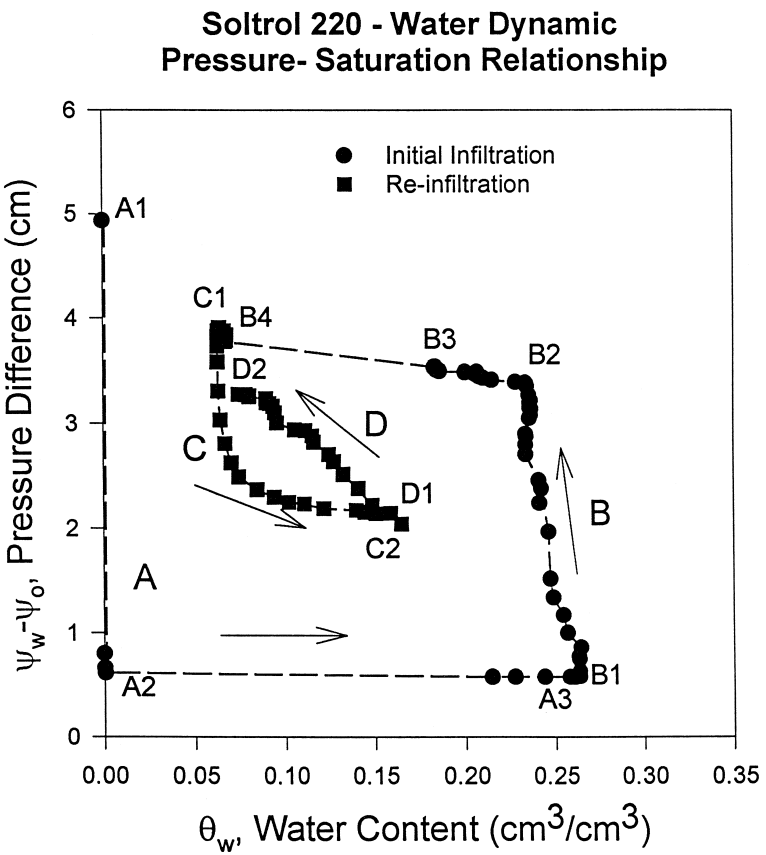

Fig. 6. Pressure–water content relationship from the finger in the 12/20 sand. (A) and (B) are the initial wetting and drying curves, and (C) and (D) are the secondary wetting and drying curves.

Taking into account the travel time between pressure and fluid content measurement location, the data in Figs. 3 and 4 are replotted to give the primary and secondary wetting loops in Fig. 6. In Fig. 6 the letter 'A' refers to the primary wetting branch beginning at A1 (oil saturated soil) via A2 (finger front starts affecting the readings) to A3 (just behind the finger tip front). Shortly after the finger tip passes the tensiometers, the pressure starts decreasing at B1 which is the starting point of the primary drying branch, 'B'. Between points B1 and B2, the matric potential decreases further while the finger remains at the high moisture content. This represents the wetted water bulb similar to the air–water systems (Selker et al., 1992b). Then, while the finger tip is moving farther down, both moisture content and matric potential are decreasing until point B3 where the water is turned off. At point B4 no water is draining out of the chamber anymore. Branches 'C' and 'D' are the wetting and drying curves during re-infiltration. Both water content and matric potential are lower in the finger tip during re-infiltration than the initial infiltration resulting in secondary wetting and drying

branches within the primary loops. All the re-infiltrations followed the second smaller hysteresis loop (only one is shown here).

The data in Fig. 6 make it possible to understand why the finger during the initial infiltration into the oil-saturated soil does expand only in the lowest portion of the tip and why the finger during re-infiltration does not go outside its confines set during the initial experiments. Sideways movement of the finger is governed by the sorptivity. Only when the sorptivity is zero will the finger not expand sideways. The sorptivity, S, can be defined as (Parlange, 1975; Brutsaert, 1976):

$$S^2 = 2\sqrt{\theta_f} \int_{\psi_{out}}^{\psi_f} \sqrt{\theta_w}\, K_w(\psi)\, d\psi \tag{14}$$

where the conductivity, $K_w(\psi)$, and the moisture content, θ_w, are functions of matric potential on the wetting branch. The integration constants are ψ_f, which is the matric potential inside the finger, and ψ_{out}, which is the potential outside the finger. Although the conductivity function is not known it is obvious that the K_w is zero when the water content is zero. Consequently, if the moisture content of the wetting curve between the integration constants is zero, we can safely assume that the sorptivity is zero too.

To examine whether the finger is expanding it is necessary to investigate the relationships of fluid contents and matric potential inside and outside the finger. For the purpose of this discussion we define the finger boundary as the locus of points just behind the wetting front at the highest matric potential. Earlier we found that for water infiltration into oil saturated sand the ψ–θ relationship outside the finger boundary is on the primary wetting loop (indicated by the 'A' segment in Fig. 6) and inside the boundary on the primary drying loop (segment 'B').

The matric potential decreases with increasing distance above the finger tip (B segment). When the matric potential within the finger, ψ_f, decreases below the value of the matric potential of point A2 (-0.75 cm in Fig. 6), the moisture content between ψ_f and ψ_{out} (both on the A segment) is zero and, hence, the sorptivity calculated in Eq. (8) becomes zero. Accordingly, anywhere in the finger with a matric potential less than -0.75 cm, the finger will not expand. Only in the region near the finger front is the finger expanding.

During re-infiltration, the water infiltrates through the previously formed finger. Within this 'old' finger the ψ–θ relationship is on the C and D segments (Fig. 6). Outside the finger the ψ–θ relationship remains on the A segment. The matric potential inside the 'old' finger never exceeds a value of -2 cm (Fig. 6) and according to the above argument the water will not cross the 'old' finger boundary. But as the moisture content and the conductivity within the 'old' finger are finite over this range of matric potential, the sorptivity is finite and the finger can expand to the 'old' finger boundaries.

These findings are important because it shows that knowledge concerning the constitutive relationships are required for hydrodynamic control in remediation sites with immiscible liquids. It also shows that when models do not include these hysteretic constitutive relationships, no realistic planning of cleanup procedures can be achieved. The difficulty is, however, that the hysteretic constitutive relations for oil–water systems are generally not known. We will investigate next if Miller and Miller (1956) scaling can be used to obtain the hysteretic constitutive relations as well as the finger diameter.

Table 2
Overview of finger experiments and parameters needed for scaling

Experiment	Type	Interfacial tension (gs^{-2})	D_{50} (mm)	Density resident fluid ($g\ cm^{-3}$)	Water content finger tip ($cm^3 \cdot cm^3$)	Observed finger diameter (cm)
This study	I	41	0.77	0.8	0.27	5.5
	II	41	0.77	0.8	0.27	5.2
	III	41	0.77	0.8	0.3	7
	IV	41	1.1	0.8	0.3	3
	V	41	1.1	0.8	0.27	3.25
	VI	41	1.1	0.8	0.2	3
Yao and Hendrickx, 1996	perlite	72	1.1	0	0.35	3
	perlite	72	0.77	0	0.35	4
	perlite	72	0.53	0	0.35	6
	perlite	72	0.34	0	0.35	10
	sand	72	1.1	0	0.35	2.5
	sand	72	0.77	0	0.35	4
	sand	72	0.53	0	0.35	6.5
Chandler et al., 1997		41	1.1	0.8	0.3	4.7
		41	0.77	0.8	0.3	4.8
Selker et al., 1992c		72	0.77	0	0.35	1.8
		72	0.53	0	0.35	3.3
Liu et al., 1994b		72	0.77	0	0.35	2.3
DiCarlo et al., 1997		72	1.1	0	0.35	1.7
		72	0.77	0	0.35	2.3

6.3. Scaling of fingers

Before we compare the observed and predicted width by scaling we will justify the scaling parameters used.

Glass et al. (1991a), Parlange et al. (1990), and Schroth et al. (1996) found that the sands in Table 2 are Miller and Miller-scale similar and can be scaled according to Eq. (8) with the mean particle sizes given in Table 2.

The scaling factor for interfacial tension, f_σ, is somewhat uncertain due to the unknown contact angle (Chandler et al., 1997) and the change of interfacial tension of oil and water in time (Schroth et al., 1995). Here we derive the scaling for interfacial tension, f_σ, by matching the soil characteristic curves of oil–water and air–water systems. This has the advantage that $\sigma_{o/w}$ includes the unknown contact angle. Schroth et al. (1996) found f_σ values between 1.6 and 1.8 by matching drainage curves in oil–water and air–water systems for different sand sizes. In Fig. 7, we compared the scaled 12/20 air–water drainage curve of Schroth et al. (1996) using $f_\sigma = 1.76$ and the sand oil–water characteristic curve (Fig. 7). The scaled soil characteristic air–water curve for 20/30 sand (Liu et al., 1994a) is also depicted. All three drainage curves are close and certainly within the experimental error of the tensiometers. The slight difference in slope between Schroth et al. (1996) and both Liu et al. (1994a) and ours is likely caused by the calculation procedure followed by Schroth et al. (1996) to correct for the changes in moisture content with elevation within the Tempe cell. The wetting curves of Liu et al. (1994a) and ours are also very close. The slight offset between the

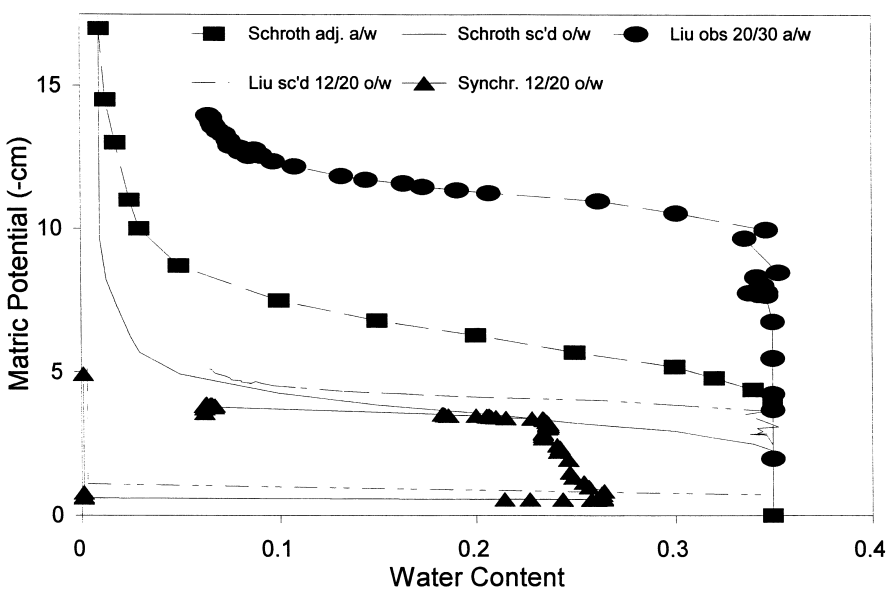

Fig. 7. Observed (obs) and scaled (sc'd) oil–water characteristic curves for Soltrol 220 and water (o/w). The scaled curves were derived from Schroth et al. (1996) and Liu et al. (1994a).

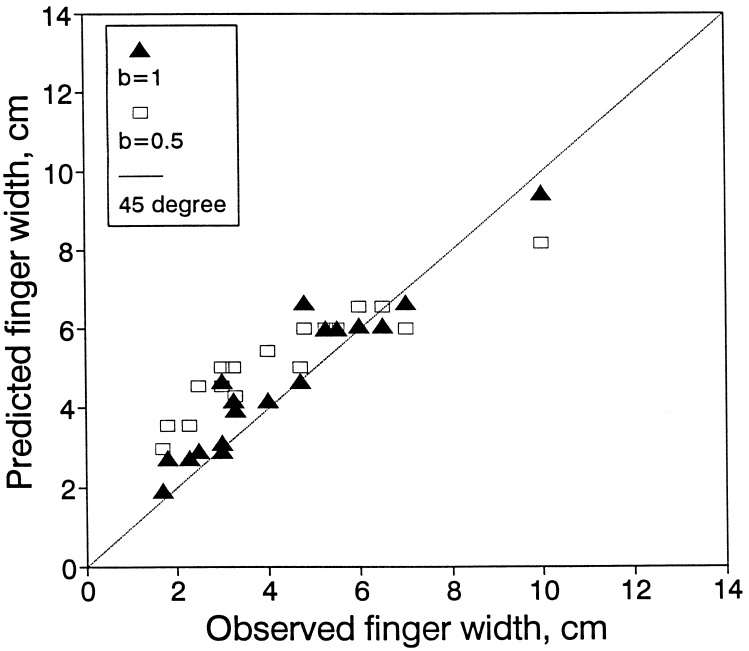

Fig. 8. Comparison of scaled finger diameter (Eqs. (7)–(11)) according to theory originally developed by Parlange and Hill (1976) ($b = 1$) and Chuoke et al. (1959) ($b = 0.5$).

two curves is either caused by the oil–water curve not going all the way to saturation or slight differences in reading the absolute pressures. Based on the above, a value of $f_\sigma = 1.76$ or an interfacial tension of 41 g s^{-2} for oil–water and 72 g s^{-2} for air–water will be used for scaling the finger diameter (Table 2).

The scaling factor for 2-d and 3-d fingers, c_κ, for air–water systems is equal to $4.8/\pi$ (Glass et al., 1990). It is the same for oil–water systems. The scaling factor, f_G, is either equal to 1 or 0.2, depending on the reference fluid.

Table 2 gives the finger diameters for a number of experiments reported in the literature. For 2-d fingers the average finger width was taken. For 3-d column experiments by Yao and Hendrickx (1996) coalescence of fingers is a problem in measuring the diameter (see their Fig. 6). The minimum finger diameter, representing a single finger, was more appropriate and is reported in Table 2.

Taking the 20/30 sand as the reference soil and oil–water as the reference liquid (average 2-d diameter is 6 cm), the finger diameters for the experiment in Table 2 were calculated with Eq. (7) for $b = 1$ and $b = 0.5$ using values of scaling factors as derived above. The predicted scaled finger diameters are compared with the observed finger diameters in Fig. 8. Note that not all moisture contents in the tips were measured and some were estimated based on similar experiments. In general, there was a satisfactory agreement between the scaled finger size and the observed value. A value of $b = 1$ (standard deviation with 45° line, $\sigma = 0.73$) gives a slightly better estimate than $b = 0.5$ ($\sigma = 1.38$).

7. Conclusions

Unstable flow experiments were carried out in slab chambers with Soltrol and water. High-intensity synchrotron radiation coupled with pressure measurements was an effective method of studying flow instabilities in oil-saturated porous media.

Hysteresis in the constitutive relations was the governing mechanism for the temporal persistence of fingered flow. Hysteresis provided the soil with a memory of previously formed finger paths.

The results show that fingered flow of water into an oil-saturated porous medium has similar properties to fingered water flow into dry porous media, but with different length scales, pressure heads, and fluid contents. Scaling of unstable flow paths might overcome some of the difficulties of measuring the constitutive relations in oil–water systems for different soils. These results will ultimately be incorporated in theories of preferential flow and, hopefully, will eventually lead to better hydrological control of in situ remediation in which immiscible fluids are a problem.

Acknowledgements

We gratefully thank Christophe Darnault, John Phillips, and Edward Zhang for their experimental assistance. This work was sponsored (in part) by the Air Force Office of Scientific Research, under grant/contract number F49620-94-1-0291. Also, the knowledgeable help of the CHESS staff is greatly appreciated.

References

Batterman, B.W., Ashcroft, N.W., 1979. CHESS: The new synchrotron radiation facility at Cornell. Science 206, 157–161.

Bierck, B.R., Wells, S., Dick, R.I., 1988. Compressible cake filtration: Monitoring cake formation and shrinkage using X-rays from a synchrotron source. J. Water Pollut. Control Fed. 60, 645–650.

Brooks, R.H., Corey, A.T., 1964. Hydraulic Properties of Porous Media. Hydrology Paper 3, Colorado State University, Fort Collins, CO, 27 pp.

Brutsaert, W.H., 1976. The concise formulation of diffuse sorption in a dry soil. Water Resources Res. 12, 1118–1124.

Chandler, D.G., Cohen, Z., Wong, E.Y., DiCarlo, D.A., Steenhuis, T.S., Parlange. J.-Y., 1997. Unstable fingered flow of water into a light oil. Submitted to Water Resources Res.

Chuoke, R.L., van Meurs, P., van der Poel, C., 1959. The instability of slow, immiscible viscous, liquid–liquid displacement in permeable media. Petrol. Trans. AIME 216, 188–194.

Conrad, S.H., Wilson, J.L., Mason, W.R., Peplinski, W.L., 1992. Visualization of residual organic liquid trapped in aquifers. Water Resources Res. 28, 467–478.

Craft, B.C., Hawkins M.F., 1959. Applied Petroleum Reservoir Engineering. Chemical Engineering Series, Prentice Hall, Englewood Cliffs, NJ.

Dane, J.H., Oostrom, M., Missildine, B.C., 1992. An improved method for the determination of capillary pressure–saturation curves involving TCE. Water and Air. J. Cont. Hydr. 11, 69–81.

Darnault, C.J.G., Throop, J.A., Rimmer, A., DiCarlo, D.A., Steenhuis, T.S., Parlange, J.-Y., 1998. Visualization by light transmission of oil and water contents in transient two-phase flow fields. J. Cont. Hydrol. 31, 335–346.

Department of Energy, 1995. Closing the Circle on Splitting the Atom: The Environmental Legacy of Nuclear Weapons Production in the United States and What DOE is Doing About It. U.S. Department of Energy, Office of Strategic Planning and Analysis, Washington, DC.

DiCarlo, D., Bauters, T.W.J., Darnault, C., Steenhuis, T.S., Parlange. J.-Y., 1997. Vapor-driven expansion of preferential flow paths. Submitted to Water Resources Res.

Glass, R.J., Parlange, J.-Y., Steenhuis, T.S., 1989a. Wetting front instability: 1. Theoretical discussion and dimensional analysis. Water Resources Res. 25 (6), 1187–1194.

Glass, R.J., Steenhuis, T.S., Parlange, J.-Y., 1989b. Wetting front instability: 2. Experimental determination of relationships between system parameters and two-dimensional unstable flow field behavior in initially dry porous media. Water Resources Res. 25 (6), 1195–1207.

Glass, R.J., Steenhuis, T.S., Parlange, J.-Y., 1989c. Mechanism for finger persistence in homogeneous, unsaturated porous media: Theory and verification. Soil Sci. 148 (1), 60–70.

Glass, R.J., Cann, S., King, J., Bailey, N., Parlange, J.-Y., Steenhuis, T.S., 1990. Wetting front instability in unsaturated porous media: A three-dimensional study in initially dry sand. Transport Porous Media J. 5, 247–268.

Glass, R.J., Orear, L., Ginn, W.C., Parlange, J.-Y., Steenhuis, T.S., 1991a. Miller Scaling of Finger Properties. American Geophysical Union–Soil Science Society of America Characterization of Transport Phenomena in the Vadose Zone Workshop, Tucson, AZ, April 2–5, 1991.

Glass, R.J., Parlange, J.-Y., Steenhuis, T.S., 1991b. Immiscible displacement in porous media: Stability analysis of three-dimensional, axisymmetric disturbances with application to gravity-driven wetting front instability. Water Resources Res. 27 (8), 1947–1956.

Glass, R.J., Nicholl, M.J., 1996. Physics of gravity fingering of immiscible fluids within a porous media. An overview of current understanding and selected complicating factors. Geoderma 70, 133–164.

Hillel, D., Baker, R.S., 1988. A descriptive theory of fingering during infiltration into layered soils. Soil Sci. 146 (1), 51–56.

Homsy, G.M., 1987. Viscous fingering in a porous media. Annu. Rev. Fluid Mech. 19, 271–311.

Hopmans, J.W., Dane, J.H., 1986. Calibration of a dual-energy gamma radiation system for multiple point measurements in a soil. Water Resources Res. 7, 1009–1114.

Lenhard, R.J., Dane, J.H., Parker, J.C., Kaluarchchi, J.J., 1988. Measurement and simulation of one-dimensional transient three-phase flow for monotonic liquid drainage. Water Resources Res. 24 (6), 853–863.

Liu, Y., Bierck, B.R., Selker, J.S., Steenhuis, T.S., Parlange, J.-Y., 1993. High intensity X-rays and tensiometer measurements in rapidly changing preferential flow fields. Soil Sci. Soc. Am. J. 57, 1188–1192.

Liu, Y., Steenhuis, T.S., Parlange, J.-Y., 1994a. Closed form solution for finger width in sandy soils at different water contents. Water Resources Res. 30 (4), 949–952.

Liu, Y., Steenhuis, T.S., Parlange, J.-Y., 1994b. Formation and persistence of fingered flow fields in coarse grained soils under different moisture contents. J. Hydr. 159, 187–195.

Mercer, J.W., Cohen, R.M., 1990. A review of immiscible fluids in the subsurface: Properties, models characterization and remediation. J. Cont. Hydr. 6, 107–163.

Miller, E.E., Miller, R.D., 1956. Physical theory for capillary flow phenomena. J. Appl. Phys. 27, 324–332.

Parker, J.C., Lenhard, R.J., 1987. A model for hysteretic constitutive relations governing multi-phase flow: 1. Saturation–pressure relations. Water Resources Res. 23, 2187–2196.

Parlange, J.-Y., 1975. On solving the flow equation in unsaturated soils by optimization: Horizontal infiltration. Soil Sci. Soc Am. J. 39, 415–417.

Parlange, J.-Y., Hill, D.E., 1976. Theoretical analysis of wetting front instability in soils. Soil Sci. 122, 236–239.

Parlange, J.-Y., Glass, R.J., Steenhuis T.S., 1990. Application of scaling to the analysis of unstable flow phenomena. In: Hillel, D., Elrick, D.E. (Eds.), Scaling in Soil Physics: Principles and Applications, Chap. 5. Soil Sci. Soc. Am. Special Pub. No. 25. pp. 53–57.

Philip, J.R., 1975. Stability analysis of infiltration. Soil Sci. Soc. Am. Proc. 39, 1042–1049.

Powers, S.E., Abriola, L.M., Weber, W.J., 1992. An experimental investigation of non-aqueous phase liquid dissolution in saturated sub-surface systems: Steady state mass transfer rates. Water Resources Res. 28, 2691–2705.

Raats, P.A.C., 1973. Unstable wetting fronts in uniform and non-uniform soils. Soil Sci. Soc. Am. Proc. 39, 1042–1049.

Saffman, P.G., Taylor, G.F.R.S., 1958. The penetration of a fluid into a porous medium or Hele–Shaw cell containing a more viscous liquid. Proc. R. Soc. London, Ser. A 246, 312–331.

Schroth, M.H., Istok, J.D., Ahearn, S.J., Selker, J.S., 1995. Geometry and position of light nonaqueous-phase liquid lenses in water-wetted porous media. J. Cont. Hydr. 19, 269–287.

Schroth, M.H., Ahearn, S.J., Selker, J.S., Istok, J.D., 1996. Characterization of Miller-similar silica sands for laboratory hydrologic studies. Soil Sci. Soc. Am. J. 60, 1331–1339.

Selker, J.S., Leclerq, P., Parlange, J.-Y., Steenhuis, T.S., 1992a. Fingered flow in two dimensions: Part 1. Measurement of matric potential. Water Resources Res. 28 (9), 2513–2521.

Selker, J.S., Leclerq, P., Parlange, J.-Y., Steenhuis, T.S., 1992b. Fingered flow in two dimensions: Part 2. Predicting finger moisture profile. Water Resources Res. 28 (9), 2523–2528.

Selker, J.S., Steenhuis, T.S., Parlange, J.-Y., 1992c. Wetting front instability in homogeneous sand soils under continuous infiltration. Soil Sci. Soc. Am. J. 56 (5), 1346–1350.

Tidwell, V.C., Glass, R.J., 1994. X-ray and visible light transmission for laboratory measurements of two-dimensional saturation fields in thin-slab systems. Water Resources Res. 30, 2873–2882.

Van Geel, P.J., Sykes, J.F., 1994. Laboratory and model simulations of a LNAPL spill in a variably-saturated sand: 1. Laboratory experiment and analysis technique. J. Cont. Hydr. 17, 1–25.

Wilkins, M.D., Abriola, L.M., Pennel, K.D., 1995. An experimental investigation of rate-limited nonaqueous phase liquid volatilization in unsaturated porous media: Steady state mass transfer. Water Resources Res. 31, 2159–2172.

Yao, T.-M., Hendrickx, J.M.H., 1996. Stability of wetting fronts in dry homogeneous soils under low infiltration rates. Soil Sci. Soc. Am. J. 60, 20–28.